Korean J. Chem. Eng., 36(9), 1527-1535 (2019)
DOI: 10.1007/s11814-019-0326-7

pISSN: 0256-1115
eISSN: 1975-7220

Comparative photocatalytic behavior of photocatalysts (TiO_2, SiC, Bi_2O_3, ZnO) for transformation of glycerol to value added compounds

Paphada Limpachanangkul*, Trin Jedsukontorn, Guoqiang Zhang***, Licheng Liu***, Mali Hunsom****, and Benjapon Chalermsinsuwan*,*****,†**

*Fuels Research Center, Department of Chemical Technology, Faculty of Science, Chulalongkorn University, Bangkok 10330, Thailand
**PTT LNG, Map ta Phut Industrial Estate, Rayong 21150, Thailand
***CAS Key Laboratory of Bio-Based Materials, Qingdao Institute of Bioenergy and Bioprocess Technology, Chinese Academy of Sciences, Qingdao 266101, Shandong, China
****Associate Fellow of Royal Society of Thailand (AFRST), Bangkok 10300, Thailand
*****Center of Excellence on Petrochemical and Materials Technology, Chulalongkorn University, Bangkok 10330, Thailand
(*Received 14 March 2019 • accepted 13 June 2019*)

Abstract−Four types of semiconductors were used as photocatalyst to convert glycerol to other value added compounds at identical testing condition in the presence of H_2O_2 as the electron acceptor. The results demonstrated that the band gap energy affected the photocatalytic activity of glycerol than the crystallite size and textural property of the utilized photocatalyst. The SiC, Bi_2O_3 and ZnO achieved almost complete glycerol conversion at 8 h of reaction time, which was significantly higher than that of TiO_2. Similar types of products, including dihydroxyacetone, glyceraldehyde, glyceric acid, glycolic acid and formic acid, were generated via all explored photocatalysts. Interestingly, one additional compound known as glyoxylic acid, an important intermediate of organic chemicals, used in medicine, spices, pesticides, paint, paper and food, was produced via Bi_2O_3. The reaction mechanism and the pathways of photocatalytic conversion of glycerol via Bi_2O_3 were proposed. Finally, the reusability of Bi_2O_3 photocatalyst was explored.

Keywords: Glycerol Conversion, Photocatalyst, Bismuth Oxide, Glyoxylic Acid, Photocatalytic

INTRODUCTION

The photocatalytic process is based on the absorption of an adequate portion of irradiated light by a catalyst or substrate, resulting in the transfer of electrons from the valence band (VB) to the conduction band (CB), leaving the photogenerated hole (h^+) with oxidation properties in the VB and photogenerated electron (e^-) with reduction properties in the CB [1,2]. The photogenerated e^- can react with O_2 to produce the anion radicals $O_2^{\bullet-}$, while the h^+ can react with H_2O to form $OH^\bullet$ radicals. Both generated species exhibit high oxidizing and reducing power, so are able to decompose or convert the organic molecules to the other molecules. Thus, the photocatalytic process is currently adopted in a wide range of applications such as disinfection in both gas and water matrices [3-5], wastewater treatment [6-9] and H_2 production by water splitting [10-13], as well as the conversion of biomass, waste or industrial by-products to value added compounds [14-18]. Among these, the use of photocatalytic process to convert biomass/waste or by-product from industrial process to high value added compounds is more interesting for sustainable development. In this context, glycerol is of interest because it contains three hydroxyl (-OH) groups, and is more reactive to convert to high value bio-based compounds. In addition, a large production rate of glycerol occurs because it is a by-product of biodiesel production. By 2018, it was expected that the biodiesel production would grow to 1.48 billion liters [19], resulting in the generation of glycerol as by-product at least 0.148 billion liters.

The photocatalytic process thus should be applied for glycerol conversion to value added compounds by TiO_2-based photocatalyst. The photocatalytic oxidation of glycerol by the home-made TiO_2 in the anatase, rutile or anatase-rutile polymorphic phases provided at least five chemical substances including 1,3-dihydroxyacetone (DHA), glyceraldehyde (GCD), formic acid (FMA) and carbon dioxide (CO_2) together with two unidentified products having molecular weights higher than that of glycerol, found as peaks at m/z 176 and m/z 268 of ESI-MS spectra [20]. The glycerol oxidation over TiO_2 photocatalyst in the presence of O_2 as electron acceptor gave CO_2 and the chemical reaction rate increased markedly in the presence of noble metal crystallites (*ex.* Pt) [21]. The transformation of glycerol to the other chemicals involved many steps, including hydrogenolysis to propylene glycol, dehydration to GCD, dehydration/dehydrogenation/decarbonylation to the formation of various reaction intermediates (e.g., glycoaldehyde, 2-oxopropanol, acetaldehyde, acetone, ethanol and methanol as well as CO_2). By using Merck TiO_2, the GCD and DHA were mainly observed as the main products, while the major products catalyzed by Degussa P25 were GCD and formaldehyde (FMD). The dissimilarity of major products between different TiO_2 specimens was principally due to the different surface morphology [22]. Also, different facets of TiO_2 loaded on different

†To whom correspondence should be addressed.
E-mail: benjapon.c@chula.ac.th

metal nanoparticles (e.g., Rh, Ru, Cu, Ni, Pt, Pd, and Au) provided different product selectivity [23]. Glycerol could be converted with high selectivity to hydroxyacetaldehyde (HAA) at about 90% on the rutile TiO_2, which have a high percentage of (110) facets, while anatase TiO_2 with dominant (101) or (001) facets provided an HAA selectivity of less than 50% and 20%, respectively. With this method, the conversion of glycerol was significantly enhanced, and the yield of hydrogen production was also greatly increased in the presence of co-catalyst. The glycerol conversion in the presence of H_2O_2 via the commercial anatase TiO_2 powder could proceed by both h^+-mediate and radical-mediated routes, but the radical-mediated route was dominant [16]. The use of H_2O_2 and O_2 as the electron acceptor enhanced the generation of both $OH^•$ radicals and $^1O_2$ in different concentrations [24]. More glycerol conversion could be achieved in the presence of H_2O_2 than O_2, but the type of generated value added compounds depended on the concentration of the generated reactivity oxidizing species (ROS), not the type of ROS.

Besides TiO_2-based photocatalyst, the photooxidation of crude glycerol using $TiSi_2$ under solar light and mild condition (60 °C and 1 atm) using *in situ* oxygen as oxidant showed 100% selectivity toward glyceric acid (GCA) in batch reaction [25]. H_2 and O_2 were also obtained in this system because the glycerol presented in the solution helped the water splitting reaction of $TiSi_2$. The glycerol was selectively oxidized to DHA with 91% selectivity at 96% conversion under visible light irradiation over Bi_2WO_6 [26]. The presence of O_2 was believed as a prime oxidant in selective oxidation of glycerol. The main ROS for selective oxidation of glycerol to DHA were the photogenerated h^+ and $O_2^{•-}$ radicals, which were generated from the band gap excitation upon visible light irradiation. The photooxidation of glycerol by $Na_4W_{10}O_{32}$ entrapped in a silica matrix favored to produce GCD and DHA with small partial degradation and selectivity of the substrate to CO_2 [27]. This is because silica surface can achieve alcohol adsorption, resulting in an improvement of the alcohol local concentration and then favor its reaction with photogenerated OH• radicals to form the both mentioned products with the CO_2 formation. The photocatalytic glycerol conversion via ZnO photocatalyst provided two principal chemicals, including GCD and DHA. The glycerol conversion and yield of both chemicals increased with increasing catalyst concentration, initial pH and reaction time [28]. The initial pH was the most significant parameter for glycerol conversion, while the temperature affected the selectivity of both GCD and DHA. In comparison with TiO_2, ZnO yielded about 16-times GCD and 2.5-times DHA higher than that of TiO_2, but TiO_2 generated a greater variety of products, such as FMD and GCAD obtained from the cleavage of the glycerol molecule [29]. In this study, the photocatalytic activity of glycerol conversion by four commercial photocatalysts including TiO_2, SiC, Bi_2O_3 and ZnO was compared. The product selectivity via each catalyst was explored and finally the mechanism of glycerol conversion by the selected Bi_2O_3 photocatalyst was proposed.

EXPERIMENTAL

1. Photocatalyst and Characterization

The photocatalytic activity for glycerol conversion to value added compounds was tested with three types of semiconductors, including SiC (Sigma-Aldrich), Bi_2O_3 (99.9%, Sigma-Aldrich) and ZnO (Sigma-Aldrich) and benchmarked with the conventionally used photocatalyst (TiO_2, Sigma-Aldrich). All the photocatalysts were dried at 105 °C for 30 min to eliminate free moisture. The diffuse reflectance spectra were measured by UV-visible near infrared spectrometry (UV-Vis; Perkin Elmer, Lambda 950) within a wavelength of 320-720 nm. The density of the state of the valence band was recorded using X-ray photoelectron spectroscopy (XPS; Axis Supra, Kratos UK) with a Delay Line detector (DLD) and a monochromatic Al Kα (hν=1,486.6 eV) source. Accurate binding energies (±0.1 eV) were established with respect to the position of the adventitious carbon C1s peak at 284.8 eV. Their crystallite structure was analyzed by the X-ray diffraction (XRD) using a D8 Discover-Bruker AXS X-ray diffractometer equipped with CuKα operated at 40 mA and 40 kV. The textural properties including BET surface area and pore size/volume of all commercial photocatalysts were characterized by the Autosorb-1 (Quantachrome).

2. Photocatalytic Activity Test

The photocatalytic activity of all commercial photocatalysts was experimented in a cylindrical glass reactor having total volume of 250 mL. In each experiment, approximately 0.3 g of the employed photocatalyst was dispersed in the 100 mL of 0.3 M glycerol ($C_3H_8O_3$, 99.5% QRec). The solution was agitated continuously by a magnetic stirrer at 400 rpm for 30 min to provide a good dispersion and equilibrium adsorption of $C_3H_8O_3$ on the photocatalyst surface. Then, approximately 15.32 mL of 30 wt% H_2O_2 was added into the glycerol solution before starting the chemical reaction. Afterward, the system was irradiated with UV light (120 W, 100-600 nm) at the light intensity of 5.93 mW/cm^2 for 8 h. As the experiment advanced, 2 mL samples were sampled and centrifuged to separate the solid catalyst from the liquid sample.

The quantitative analysis of glycerol and generated chemical species was characterized by high performance liquid chromatography (HPLC) with an RID-10A refractive index detector (Shimadzu). The stationary phase was aminex HPX-87H ion exclusion (300 mm×7.8 mm), and the mobile phase was an acetonitrile-water solution (70 : 30 V/V) with 5 mM H_2SO_4 at a constant flow rate of 0.4 mL/min standard solutions of glycerol and expected major product compounds including DHA ($C_3H_6O_3$, Sigma Aldrich), GCD ($C_3H_6O_3$, Sigma Aldrich), GCA ($C_3H_6O_4$, Sigma Aldrich), glycolic acid ($C_2H_4O_3$, GCOA, Sigma Aldrich), glyoxylic acid ($C_2H_2O_3$, GOX, Sigma Aldrich) and formic acid ($C_2H_4O_3$, FMA, Sigma Aldrich) were used to define the relationship between the peak area and concentration [16]. The glycerol conversion (X) and product selectivity (S) obtained from the reaction were computed, respectively, according to Eqs. (1) and (2):

$$X_{GLY}(\%) = \frac{\text{amount of glycerol converted}}{\text{Total amount of glycerol in reactant}} \times 100\% \quad (1)$$

$$S(\%) = \frac{\text{amount of desired product j formed}}{\text{amount of all products formed}} \times 100\% \quad (2)$$

RESULTS AND DISCUSSION

1. Property of Photocatalysts

The light absorption capability of all photocatalysts is exhibited

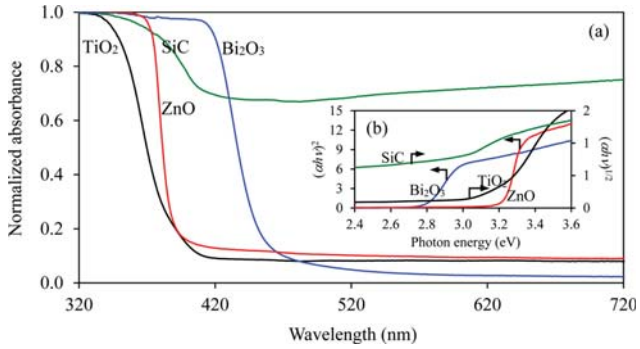

Fig. 1. (a) UV-visible spectra and (b) the depended of $(\alpha h\nu)^{1/n}$ on photon energy of the selected photocatalysts.

in Fig. 1(a). It was obviously revealed that both TiO_2 and ZnO exhibited the absorption capability under the UV light region (λ< 380 nm) and dropped drastically to a zero value under the visible light region (λ>380 nm), suggesting their visible light inactivity. The Bi_2O_3 photocatalyst exhibited absorption ability for both UV light and short-wavelength visible light (380<λ<420) regions. However, the absorption spectrum of SiC was still detected in both UV- and visible light regions, suggesting its ability to absorb both UV- and visible light. The band gap energy of all commercial photocatalysts was estimated from the Tauc's plot, the plot of $(\alpha h\nu)^{1/n}$. Typically, the transitions dominate the basic absorption processes, giving either n=1/2 or n=2, for direct and indirect transitions, respectively. Thus, n is 2 for TiO_2 and SiC and n=1/2 for ZnO and Bi_2O_3 [30-33] and $h\nu$ of the linear portion of the fundamental absorption edge of the UV-Vis spectra (Fig. 1(b)) [34]. As summarized in Table 1, the band gap values of TiO_2≈ZnO>Bi_2O_3>SiC.

To explore the electron density state of the valence band of the photocatalysts, the valence band XPS was evaluated. The TiO_2, SiC, Bi_2O_3 and ZnO photocatalyst powders showed a typical valence band with the edge of the maximum energy at around 2.23, 1.63, 1.75 and 2.59 eV, respectively (Fig. 2), consistent with the previous works [35-38]. However, the band gap energies of TiO_2, SiC, Bi_2O_3 and ZnO were 3.18, 2.62, 2.82 and 3.23 eV, suggesting that the

Table 1. Property of selected photocatalysts

Photocatalyst	Band gap energy (eV)	Crystallite size (nm)	Textural property			
			BET surface area (m^2/g)	Pore volume (cm^3/g)		Average pore size (°A)
				Micropore volume	Mesopore volume	
TiO_2	3.18	50.89	15.95	0.0164	0.0558	123
SiC	2.62	52.15	13.46	0.0126	0.0290	65.7
Bi_2O_3	2.82	72.62	3.15	0.0027	0.0065	61.5
ZnO	3.23	31.54	17.69	0.0189	0.0589	129

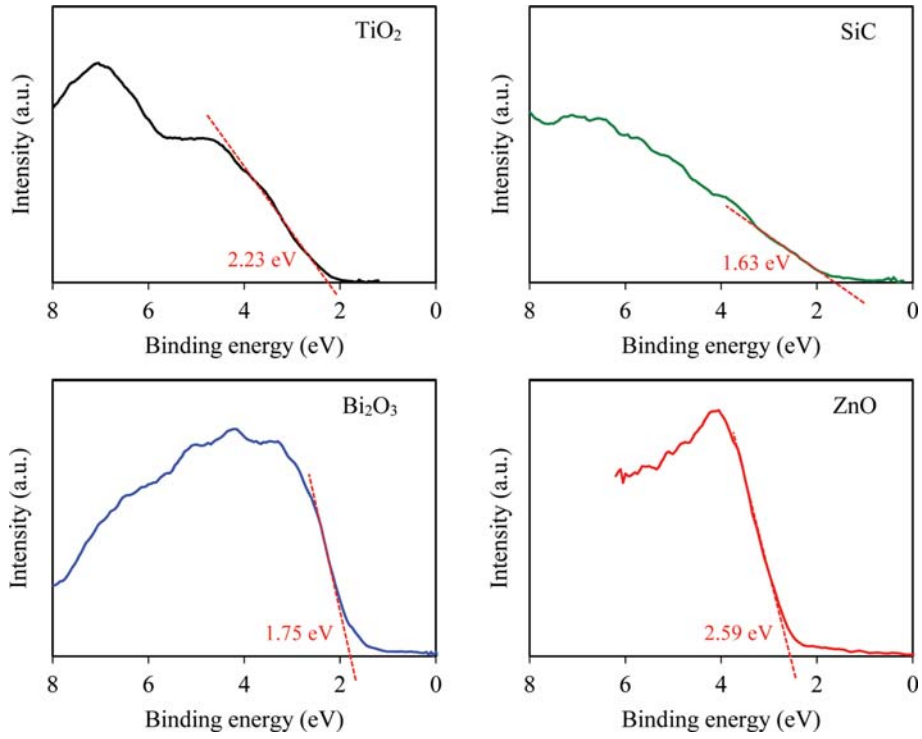

Fig. 2. Valence band spectra of the selected photocatalysts.

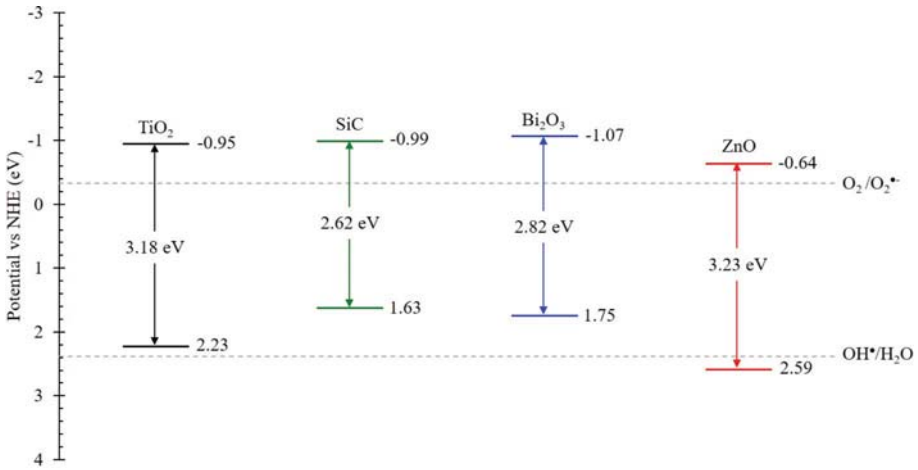

Scheme 1. Energy band positions of the photocatalysts and their band gap energies.

minimum conduction band would occur at –0.95, –0.99, –1.07 and –0.64 eV, respectively. As shown in Scheme 1, the tops of the valence bands of the semiconductors were positioned more positively than the oxidation potential of the oxygen molecule that could be further oxidized to form anion radical $O_2^{\bullet-}$. However, only the top of the valence band of ZnO was positioned more positively than the oxidation potential of the water molecule that could be oxidized to form $OH^{\bullet}$ radicals. This suggested that the $O_2^{\bullet-}$ radicals could be generated in all investigated photocatalysts, while the $OH^{\bullet}$ radicals could be formed only in the presence of ZnO photocatalyst.

The crystal structures of all photocatalysts were analyzed as shown in Fig. 3. The XRD spectra of TiO_2 exhibited the peaks of anatase phase at 2θ position of 25.38° and 48.12°, corresponding to the crystal planes of (101) and (200), respectively [39]. The characteristic peaks of SiC powder were well exhibited for the scan angles of 34.12°, 35.68°, 38.15°, 41.41° and 60.07°, corresponding to the hexagonal polytype SiC (101), (102), (103), (104) and (110), respectively [40]. The main characteristic peaks observed from the XRD spectra of Bi_2O_3 at 2θ of 25.49°, 26.96°, 27.43°, 33.29° and 46.36° were consistent with α monoclinic phase of Bi_2O_3 (002), (111), (120), (200), (041) lattice planes, respectively [41]. The XRD spectra of ZnO showed the main peaks at the scan angle of 34.17°, 34.40°, 36.22°, 47.47°, 56.55°, 62.83° and 67.94°, assigned to the wurtzite phase of ZnO (100), (002), (101), (102), (110), (103) and (112), respectively [42]. The average grain size of all commercial photocatalyst nanoparticles was estimated from the XRD line broadening measurement using Scherrer's equation at the crystallite planes of TiO_2(101), SiC(102), Bi_2O_3(120) and ZnO(101) and summarized in Table 1. The crystallite size of utilized photocatalysts was ranked as the order of Bi_2O_3>SiC>TiO_2>ZnO. Regarding the textural properties of all photocatalysts, as shown in Fig. 4, all investigated photocatalysts revealed the features of multi-modal porous structures and absence of macropores (>50 nm). As demonstrated in Fig. 5 and Table 1, the BET surface area, pore size, micropore

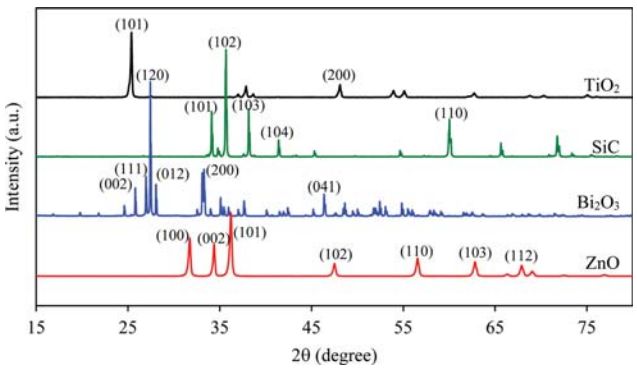

Fig. 3. Representative XRD patterns of the selected photocatalysts.

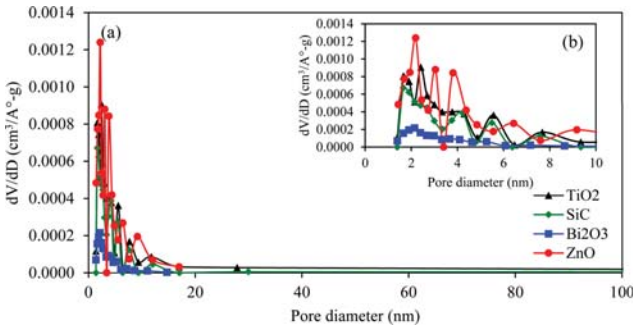

Fig. 4. (a) Pore size distribution curves and (b) a magnified pore size distribution of the selected photocatalysts.

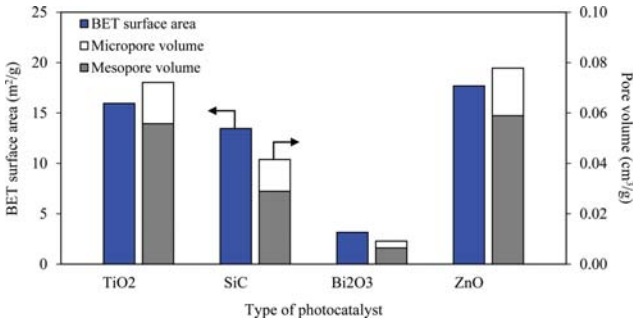

Fig. 5. Representative textural property of the selected photocatalysts.

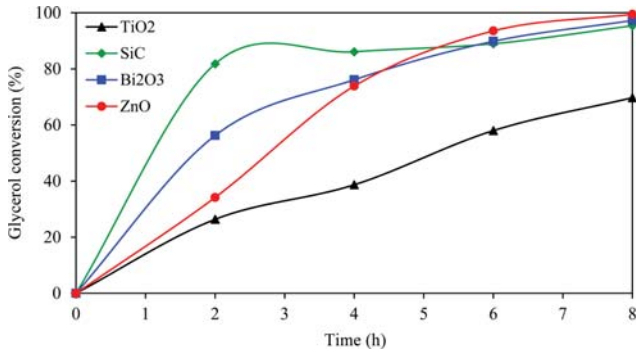

Fig. 6. Glycerol conversion as a function of time in the presence of the photocatalysts.

and mesopore volume of all photocatalysts provided a consistent trend, which can be ranked as the order of $ZnO>TiO_2>SiC>Bi_2O_3$.

2. Photocatalytic Activity Test

The photocatalytic activity of all utilized photocatalysts was found through glycerol conversion to value added compounds. As displayed in Fig. 6, the conversion of glycerol increased with the increasing reaction time at identical testing condition of photocatalyst dosage of 3 g/L, light intensity of 5.93 mW/cm^2 and reaction time of 8 h, which can be ranked in the order of $ZnO>Bi_2O_3\approx SiC>TiO_2$. The different photocatalytic activity for glycerol conversion in the presence of each photocatalyst might be attributed to their differential morphology as well as optical property. As reported elsewhere, photocatalysts with low band gap energy are capable of absorbing visible light higher than those with high band gap energy because it requires low energy to excite the electron from VB to CB [43,44]. In addition, it is believed that the photocatalyst with small crystallite size usually exhibits a large surface area, which can improve the photocatalytic activity by an increasing in the amount of reactant adsorption site. Besides, a small crystallite photocatalyst can promote the fast transport of photogenerated e^- and h^+ from the bulk to the surface [45,46], which consequently extends the e^--h^+ pair life. Also, to achieve a redox reaction, the bottoms of the conduction bands must be located at a more negative potential than the reduction potential of the chemical species that will be reduced, while the tops of the valence bands must be positioned more positively than the oxidation potential of the chemical species that will be oxidized [47]. In this study, TiO_2 exhibited the lowest photocatalytic activity for glycerol conversion, probably due to its high band gap energy (3.18 eV) and large crystallite size (50.89 nm). Although the Bi_2O_3 had high crystallite size and low textural property in comparison with SiC, it displayed the photocatalytic activity for glycerol conversion close to that of SiC, probably attributed to their close band gap energy. Moreover, only the top of the valence band of ZnO was positioned more positively than the oxidation potential of the water molecule that could be oxidized to form $OH^\bullet$ which could oxidize the glycerol molecule and provide the highest photocatalytic activity for glycerol conversion. However, the H_2O_2 can break down to form $OH^\bullet$ radicals when it absorbs UV light and makes other photocatalyst systems also have $OH^\bullet$ radicals to oxidize glycerol [48]. This suggests that the band gap energy and valence band position affected the photocatalytic activity of

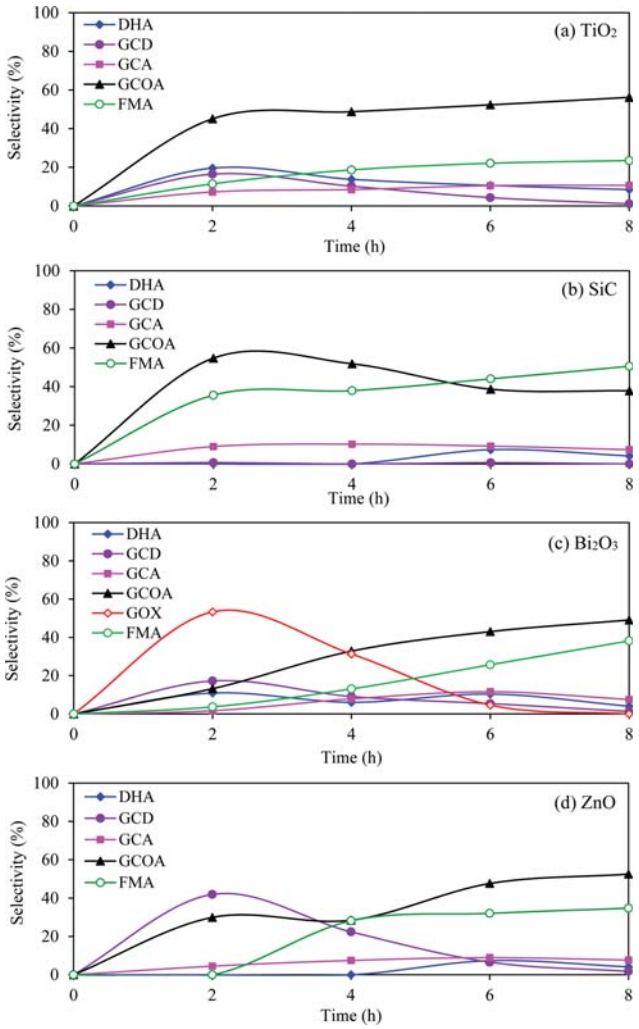

Fig. 7. Selectivity of generated compounds from glycerol conversion in the presence of the photocatalysts with light intensity of 5.93 mW/cm^2 and photocatalyst dosage of 3 g/L in the presence of H_2O_2 as electron acceptor.

glycerol conversion than the crystallite size and textural property. For ZnO, interestingly, although it had the highest band gap energy (3.23 eV) it exhibited a rapid increased rate of glycerol conversion after 3 h in comparison with other photocatalysts. This is attributed to the dissolution of ZnO particles in acidic aqueous solutions in the glycerol solution along the reaction [49], resulting in the process of glycerol conversion as the homogeneous chemical reaction.

With regard to the type of detectable generated compounds, as shown in Fig. 7, the photocatalytic conversion of glycerol by TiO_2, SiC and ZnO provided a similar type of generated product, including DHA, GCD, GCA, GCOA and FMA. The product selectivity was more pronounced for GCOA for all mentioned photocatalysts. The mechanism of glycerol conversion to DHA, GCD, GCA, GCOA and FMA by photocatalytic oxidation in the presence of H_2O_2 has already been proposed [16,50]. When the UV light irradiates the system, the electron will be excited from the VB to CB leaving the photogenerated h^+, which are able to attach the H_2O_2 to form the $OH^\bullet$ and $O_2^{\bullet-}$ radicals [24]. Meanwhile, the H_2O_2 molecule can

break down to OH• radicals [48,51]. Both $O_2^{\bullet-}$ and OH• radicals are recognized as strong oxidizing agent that are able to attach the 1° and 2° carbon atoms of glycerol molecule to form GCD or DHA, respectively. They can further oxidize the generated GCD to form GCA as well as break down the C-C bond of GCA to form GCOA [52,53].

For Bi_2O_3 photocatalyst, besides all mentioned five generated compounds, one more product named GOX was more pronounced up to the selectivity of 53.3% at the second hour of reaction time. This chemical, which is the simplest aldehyde acid, is an intermediate of organic chemicals, used in spices, pesticides, medicine, paper, food additives, paint and others [54]. Previously, it was reported that the GOX can be obtained from the selective oxidation of the primary -OH groups of glycerol to form -CHO, yielding GCD as intermediates. The generated -CHO group is very reactive which is readily selectively oxidized to GCA. The generated GCA can further oxidize to tartronic acid and then to GCOA and GOX in a separate route [55]. However, another different mechanism was also proposed that the GCA was directly converted to GCOA and then to GOX, respectively, depending on the reaction conditions and the catalyst properties [56]. In this study, tartronic acid was not generated and the generation of GOX was more pronounced at early reaction period and abated at the end. This suggested that the GOX might be not specifically obtained from the oxidation of GCOA via Bi_2O_3 photocatalyst.

To explore the route of GOX formation, all generated compounds, including DHA, GCD, GCA, GCOA and GOX, were used as the initial chemical substances and subjected to the photocatalytic reaction via Bi_2O_3 at the dosage of 3 g/L and light intensity of 5.93 mW/cm^2 in the presence of H_2O_2. As shown in Table 2, DHA converted to a huge quantity of GCOA and GOX with a trace of FMA, but not to GCD. Likewise, GCD converted to large amount of GOX and low amount of GCA, GOX and FMA, but not to DHA. This suggests that the delocalization of the -CHO group from 1°-C to 2°-C of the intermediate C_3 molecule was not achieved for the photocatalytic oxidation of glycerol via Bi_2O_3 photocatalyst, not similar to that of TiO_2 [17]. GCA principally converted to GOX and GCOA and a trace of FMA, while both GCOA and GOX converted to specifically to FMA.

The reaction mechanisms of glycerol conversion to DHA and GCD, DHA to GCOA, GCD to GCA and GCA to GCOA were already drawn previously. Briefly, HO• radicals can readily attach the 1°-C and 2°-C atom of glycerol to form GCD and DHA, respectively. The generated GCD can be further oxidized via the HO• radicals to GCA and the DHA can be oxidized to GCOA. An excess HO• radical can also attach and cleave the C-C bond of GCA, resulting in the formation of GCOA and FMA [16]. Thus, the reaction mechanism of the GOX generation from glycerol, DHA, GCD, GCA was proposed as the following. Because, the selectivity of GOX was more pronounced at the second hour of the photocatalytic oxidation of glycerol via Bi_2O_3. It was speculated that the glycerol might be directly transformed to GOX. In that case, an excess OH• radical and O_2 were sequentially attached the 1°-C atom of glycerol, leading to the cleavage of the C-C bond, resulting in the formation of GOX according to Eqs. (3)-(9).

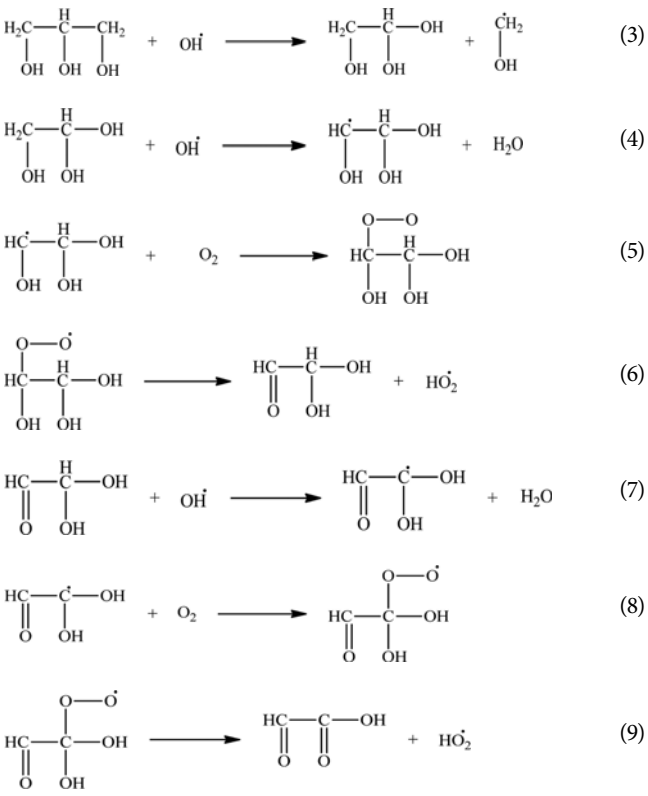

(3)

(4)

(5)

(6)

(7)

(8)

(9)

By using DHA as the initial chemical, the 1°-C atom of DHA was attached from the HO• radicals and free O_2 leading to the loss of two H atoms yielding the hydroxypyruvaldehyde ($C_3H_4O_3$) as intermediate compound (Eqs. (10)-(12)). This intermediate species was readily attached by an excess HO• radicals resulting in the cleavage of its C-C bond to form GOX and methanediol (CH_4O_2) (Eqs. (13)-(14)). Both hydroxypyruvaldehyde and methanediol were not detected in the HPLC analysis, probably caused by the limita-

Table 2. Photocatalytic catalytic conversions of glycerol, DHA, GCD, GCA, GCOA and GOX towards the known products for 2 h

Raw chemicals	Conversion (%)	C-balance (%)	Selectivity (%)					
			DHA	GCD	GCA	GCOA	GOX	FMA
GLY	56.3	98.1	10.9	17.2	1.67	13.2	53.3	3.70
DHA	100	92.6			-	45.3	48.4	6.3
GCD	100	98.0			2.8	13.8	75.7	7.8
GCA	89.3	77.0			-	22.2	68.1	9.7
GCOA	66.7	64.8			-	-	-	100
GOX	11.2	96.6			-	-	-	100

tions of the utilized column. The carbon balance (C-balance) calculated as the percentage of carbon accounted for the desired liquid products attained more than 92%, indicating that less than 8% of carbon was converted to undetectable products.

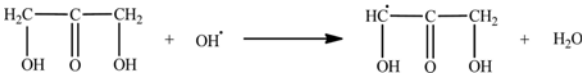
(10)

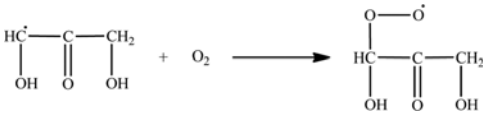
(11)

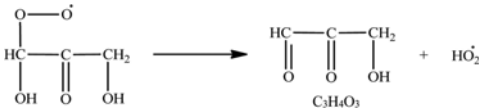
(12)

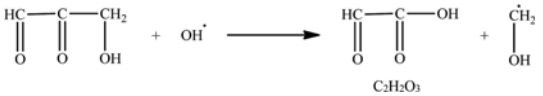
(13)

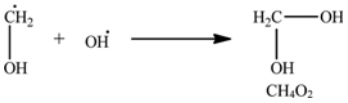
(14)

For GCD, both HO• radicals and free O_2, respectively, attached the 2°-C atom to form an intermediate $C_3H_4O_3$ species (Eqs. (15)-(17)), which then reacted with and excess HO• radicals to form GOX and CH_4O_2 as Eqs. (18)-(19). The carbon conversion was around 77%, indicating that approximately 23% of C atom in GCD molecule converted to undetectable products such as CH_4O_2.

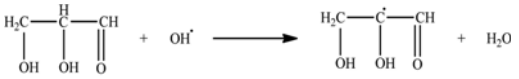
(15)

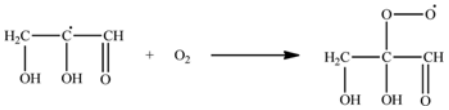
(16)

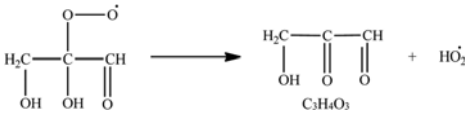
(17)


(18)

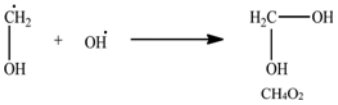
(19)

In case of GCA, its 2°-C atom was attached by the HO• radicals and free O_2 according to Eqs. (20)-(22) to form the $C_3H_4O_3$ as intermediate compound, which readily reacted with H_2O molecule to form GOX and CH_4O_2 as Eq. (23). A high carbon conversion of up to 98% was obtained in this case.

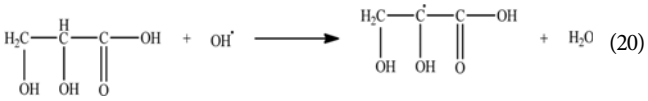
(20)

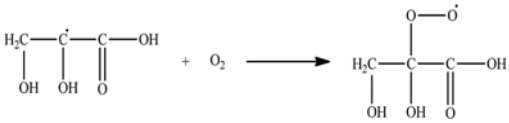
(21)

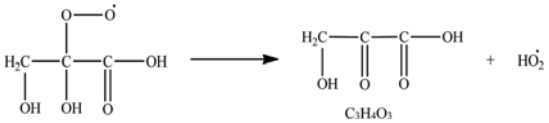
(22)

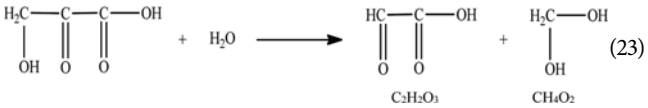
(23)

According to the obtained results and literature, the pathway of glycerol conversion as well as the product compounds by Bi_2O_3 photocatalysis in the presence of H_2O_2 is demonstrated in Scheme

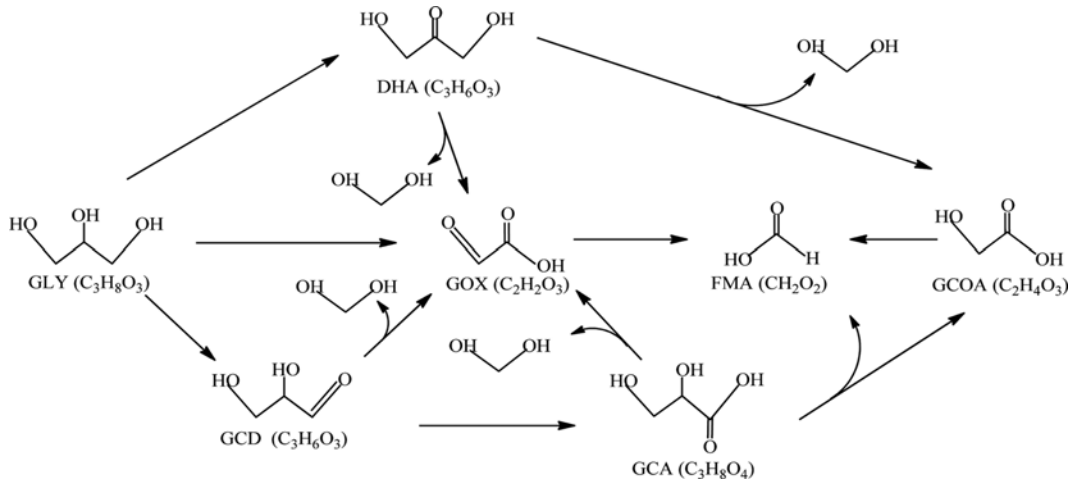

Scheme 2. Proposed reaction pathways of photocatalytic conversion of glycerol via Bi_2O_3.

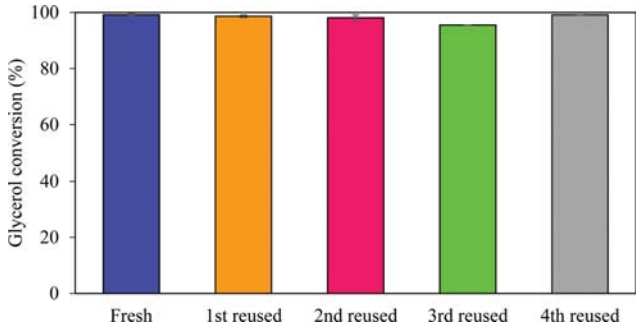

Fig. 8. Reusability of Bi_2O_3 with light intensity of 5.93 mW/cm^2 and photocatalyst dosage of 3 g/L in the presence of H_2O_2 as electron acceptor.

2. GOX can be directly obtained from glycerol, DHA, GCD and GCA.

3. Reusability of Bi_2O_3

Photocatalyst reusability in multiple photocatalytic cycles was performed with the used Bi_2O_3 at loading of 3.0 g/L suspended in 100 mL of a 0.3 M aqueous glycerol solution with an average light intensity of 5.93 mW/cm^2. Prior to the experiment, the employed photocatalyst was rinsed several times with distilled water and dried at 105 °C overnight. Fig. 8 illustrates glycerol conversion at various reusable cycles. As shown, only little change of glycerol conversion was observed after four-fold reuse. This suggests that the Bi_2O_3 photocatalyst has high stability and is able to be reused at least four times.

CONCLUSION

The photocatalytic behavior of photocatalysts, including TiO_2, SiC, Bi_2O_3, ZnO, was tested comparatively for glycerol transformation to other value added compounds at atmospheric temperature and pressure. TiO_2 exhibited the lowest photocatalytic activity for glycerol conversion in comparison with other explored photocatalysts due to its large crystallite size and high band gap energy. Bi_2O_3 had high crystallite size and low textural property in comparison with SiC, but it displayed photocatalytic activity for glycerol conversion close to that of SiC, due to their close band gap energy. The ZnO exhibited a fast increased rate of glycerol conversion after 3 h in comparison with other commercial photocatalysts, although it had the highest band gap energy, attributed to the dissolution of ZnO particles in the glycerol solution along the reaction. Similar types of generated products, including DHA, GCD, GCA, GCOA and FMA, were generated via all explored photocatalysts. Besides, one additional compound known as GOX was produced via Bi_2O_3 photocatalyst, which was principally produced from the C-C cleavage of glycerol, DHA, GCD and GCA molecules. The Bi_2O_3 photocatalyst showed high stability and can be reused for at least four cycles.

ACKNOWLEDGEMENTS

The authors would like to thank the Royal Golden Jubilee Ph.D. Program of the Thailand Research Fund (PHD/0241/2558) and the Embassy of France in Thailand for financial support.

REFERENCES

1. G. Sadanandam, K. Lalitha, V. D. Kumari, M. V. Shankar and M. Subrahmanyam, *Int. J. Hydrogen Energy*, **38**, 9655 (2013).
2. M. Stelmachowski, M. Marchwicka, E. Grabowska and M. Diak, *J. Adv. Oxidation Technologies*, **17**, 167 (2014).
3. A. Markowska-Szczupak, P. Rokicka, K. Wang, M. Endo, A. Morawski and E. Kowalska, *Catalysts*, **8**, 316 (2018).
4. K. Ouyang, K. Dai, S. L. Walker, Q. Huang, X. Yin and P. Cai, *Scientific Reports*, **6**, 25702 (2016).
5. A. Rahmani, M. Samarghandi, M. Samadi and F. Nazemi, *J. Res. Health Sci.*, **9**, 1 (2009).
6. M. I. Badawy, M. Y. Ghaly and M. E. Ali, *Desalination*, **267**, 250 (2011).
7. F. H. Hussein and T. A. Abass, *Int. J. Chem. Sci.*, **8**, 1353 (2010).
8. S. Lodha, A. Jain and P. B. Punjabi, *Arab. J. Chem.*, **4**, 383 (2011).
9. Q. Zhang, D. D. Zheng, L. S. Xu and C.-T. Chang, *Catal. Today*, **274**, 8 (2016).
10. N. A. Barakat, E. Ahmed, M. T. Amen, M. A. Abdelkareem and A. Farghali, *Mater. Lett.*, **210**, 317 (2018).
11. Y. H. Li, Y. Wang, L. R. Zheng, H. J. Zhao, H. G. Yang and C. Li, *Appl. Catal. B: Environ.*, **209**, 247 (2017).
12. J. Luan and J. Chen, *Materials*, **5**, 2423 (2012).
13. S. G. Sanches, J. H. Flores and M. I. P. da Silva, *Mater. Res. Bull.*, **109**, 82 (2019).
14. L. Da Vià, C. Recchi, E. O. Gonzalez-Yanez, T. E. Davies and J. A. Lopez-Sanchez, *Appl. Catal. B: Environ.*, **202**, 281 (2017).
15. A. Hameed, I. M. Ismail, M. Aslam and M. Gondal, *Appl. Catal. A: Gen.*, **470**, 327 (2014).
16. T. Jedsukontorn, V. Meeyoo, N. Saito and M. Hunsom, *Chem. Eng. J.*, **281**, 252 (2015).
17. T. Jedsukontorn, T. Ueno, N. Saito and M. Hunsom, *J. Alloys Compd.*, **757**, 188 (2018).
18. B. Jin, G. Yao, X. Wang, K. Ding and F. Jin, *ACS Sustainable Chem. Eng.*, **5**, 6377 (2017).
19. S. Preechajan and P. Prasertsri, *Thailand Biofuels Annual* (2017).
20. V. Augugliaro, H. H. El Nazer, V. Loddo, A. Mele, G. Palmisano, L. Palmisano and S. Yurdakal, *Catal. Today*, **151**, 21 (2010).
21. P. Panagiotopoulou, E. E. Karamerou and D. I. Kondarides, *Catal. Today*, **209**, 91 (2013).
22. C. Minero, A. Bedini and V. Maurino, *Appl. Catal. B: Environ.*, **128**, 135 (2012).
23. R. Chong, J. Li, X. Zhou, Y. Ma, J. Yang, L. Huang, H. Han, F. Zhang and C. Li, *Chem. Commun.*, **50**, 165 (2014).
24. T. Jedsukontorn, V. Meeyoo, N. Saito and M. Hunsom, *Chinese J. Catal.*, **37**, 1975 (2016).
25. N. Kondamudi, M. Misra, S. Banerjee, S. Mohapatra and S. Mohapatra, *Appl. Catal. B: Environ.*, **126**, 180 (2012).
26. Y. Zhang, N. Zhang, Z.-R. Tang and Y.-J. Xu, *Chem. Sci.*, **4**, 1820 (2013).
27. A. Molinari, A. Maldotti, A. Bratovcic and G. Magnacca, *Catal. Today*, **206**, 46 (2013).
28. N. A. Hermes, A. R. Corsetti, A. S. Pacheco and M. A. Lansarin, *J. Adv. Oxidation Technologies*, **18**, 315 (2015).
29. N. A. Hermes, A. Corsetti and M. A. Lansarin, *Chem. Lett.*, **43**, 143 (2014).

30. B. D. Viezbicke, S. Patel, B. E. Davis and D. P. Birnie III, *Physica Status Solidi*, **252**, 1700 (2015).
31. T. Subramanyam, V. Nagendra, P. Goutham and K. Subramanya, *Microelectron. Solid State Electronics*, **5**, 14 (2016).
32. E. Vasilaki, D. Vernardou, G. Kenanakis, M. Vamvakaki and N. Katsarakis, *Appl. Phys. A*, **123**, 231 (2017).
33. T. Saison, N. Chemin, C. Chanéac, O. Durupthy, V. Ruaux, L. Mariey, F. o. Maugé, P. Beaunier and J.-P. Jolivet, *J. Phys. Chem. C*, **115**, 5657 (2011).
34. A. Murphy, *Solar Energy Mater. Solar Cells*, **91**, 1326 (2007).
35. J. Ren-Xu, D. Lin-Peng, N. Ying-Xi, L. Cheng-Zhan, S. Qing-Wen, T. Xiao-Yan, Y. Fei and Z. Yu-Ming, *Chinese Phys. B*, **24**, 038103 (2015).
36. H.-Y. Jiang, G. Liu, T. Wang, P. Li, J. Lin and J. Ye, *RSC Adv.*, **5**, 92963 (2015).
37. Y. Zhang, G. Han, H. Wu, X. Wang, Y. Liu, J. Zhang, H. Liu, H. Zheng, X. Chen and C. Liu, *Nanoscale Res. Lett.*, **13**, 237 (2018).
38. J. Wang, M. Qin, H. Tao, W. Ke, Z. Chen, J. Wan, P. Qin, L. Xiong, H. Lei and H. Yu, *Appl. Phys. Lett.*, **106**, 121104 (2015).
39. S. K. Kansal, S. Sood, A. Umar and S. Mehta, *J. Alloys Compd.*, **581**, 392 (2013).
40. C. Ma, J. Yan, P. Liu, Y. Wei and G. Yang, *J. Mater. Chem. C*, **4**, 6063 (2016).
41. S. Sood, A. Umar, S. K. Mehta and S. K. Kansal, *Ceram. Int.*, **41**, 3355 (2015).
42. M. R. Arefi and S. Rezaei-Zarchi, *Int. J. Mol. Sci.*, **13**, 4340 (2012).
43. S. Anandan, Y. Ikuma and K. Niwa, *Solid State Phenomena*, **162**, 239 (2010).
44. J. Huo, Y. Hu, H. Jiang and C. Li, *Nanoscale*, **6**, 9078 (2014).
45. F. Amano, K. Nogami, M. Tanaka and B. Ohtani, *Langmuir*, **26**, 7174 (2010).
46. H. Kominami, S.-y. Murakami, J.-i. Kato, Y. Kera and B. Ohtani, *J. Phys. Chem. B*, **106**, 10501 (2002).
47. M. d. O. Melo and L. A. Silva, *J. Brazilian Chem. Soc.*, **22**, 1399 (2011).
48. G. F. Ijpelaar, D. J. Harmsen, M. Heringa and W. Kiwa, *Environ. Eng. Sci.*, **4**, 51 (2007).
49. D. J. Wesolowski, P. Bénézeth and D. A. Palmer, *Geochim. Cosmochim. Acta*, **62**, 971 (1998).
50. S. Demirel-Gülen, M. Lucas and P. Claus, *Catal. Today*, **102**, 166 (2005).
51. C. Hofman-Caris and E. Beerendonk, New concepts of UV/H_2O_2 oxidation, KWR Watercycle Research Institute, Nieuwegein, the Netherlands (2011).
52. S. Carrettin, P. McMorn, P. Johnston, K. Griffin, C. J. Kiely and G. Hutchings, *Phys. Chem. Chem. Phys.*, **5**, 1329 (2003).
53. S. Gil, M. Marchena, L. Sánchez-Silva, A. Romero, P. Sánchez and J. L. Valverde, *Chem. Eng. J.*, **178**, 423 (2011).
54. S. X. Zhang, *Adv. Mater. Res.*, **573-574**, 145 (2012).
55. C. Xu, Y. Du, C. Li, J. Yang and G. Yang, *J. Adv. Oxidation Technologies*, **164**, 334 (2015).
56. C.-H. Zhou, J. N. Beltramini, C.-X. Lin, Z.-P. Xu, G. M. Lu and A. Tanksale, *Catal. Sci. Technol.*, **1**, 111 (2011).